

Neutrino trapping and out-of-equilibrium effects in binary neutron star merger remnants

Pedro L. Espino,^{1,2} Peter Hammond,¹ David Radice,^{1,3,4} Sebastiano Bernuzzi,⁵

Rossella Gamba,⁵ Francesco Zappa,⁵ Luís Felipe Longo Micchi,⁵ and Albino Perego^{6,7}

¹*Institute for Gravitation & the Cosmos, The Pennsylvania State University, University Park PA 16802, USA*

²*Department of Physics, University of California, Berkeley, CA 94720, USA*

³*Department of Physics, The Pennsylvania State University, University Park PA 16802, USA*

⁴*Department of Astronomy & Astrophysics, The Pennsylvania State University, University Park PA 16802, USA*

⁵*Theoretisch-Physikalisches Institut, Friedrich-Schiller-Universität Jena, 07743, Jena, Germany*

⁶*Dipartimento di Fisica, Università di Trento, Via Sommarive 14, 38123 Trento, Italy*

⁷*INFN-TIFPA, Trento Institute for Fundamental Physics and Applications, via Sommarive 14, I-38123 Trento, Italy*

(Dated: November 2, 2023)

We study out-of-thermodynamic equilibrium effects in neutron star mergers with 3D general-relativistic neutrino-radiation large-eddy simulations. During merger, the cores of the neutron stars remain cold ($T \sim$ a few MeV) and out of thermodynamic equilibrium with trapped neutrinos originating from the hot collisional interface between the stars. However, within $\sim 2\text{--}3$ milliseconds matter and neutrinos reach equilibrium everywhere in the remnant. Our results show that dissipative effects, such as bulk viscosity, if present, are only active for a short window of time after the merger.

Introduction.— Neutrino interactions are expected to have profound implications for the multimessenger signals associated with binary neutron star (BNS) mergers. Not only do we expect significant neutrino luminosities from BNS mergers [1–13] but neutrinos may also have a significant impact on the properties of other BNS merger observables such as kilonovae (KN) and gravitational waves (GWs). For example, the conditions following a BNS merger allow for short-enough neutrino mean free paths to result in significant neutrino re-absorption into the medium. Such re-absorption is expected to result in the systematic increase of the average electron fraction of the post-merger disk and ejecta [7, 13–16], thereby affecting the r-process nucleosynthetic yields and subsequently the KN properties [16–20]. While eventually neutrinos stream away from the system on the diffusion timescale, they can be temporarily considered as trapped if the diffusion timescale becomes much larger than the dynamical timescale. If production and absorption reactions are fast enough, they can equilibrate with matter inside the system. The timescale for neutrino interactions may be commensurate with that of the local fluid dynamics (i.e., local fluid compression/rarefaction driven by oscillations of the post-merger remnant massive neutron star (RMNS)) [21–24]. It has been suggested that the dissipative, out-of-equilibrium effects in the matter-neutrino mixture produced in mergers may result in significant bulk-viscous damping of the post-merger oscillations of the RMNS [21–28] and, in turn, of the post-merger GW amplitude [28]. Microphysical neutrino interactions are a key ingredient in BNS mergers and must be considered for a full picture of the relevant astrophysical phenomena and, crucially, the re-absorption of neutrinos must be accurately modeled [16, 29]. To this end, moment-based neutrino transport schemes are well-suited to capturing the aforementioned phenomena, as

they provide an accurate method for capturing the effects of neutrino re-absorption in the medium across all opacity regimes [4, 30–32].

In this work we study the effect of trapped neutrinos in the core of the RMNSs on the local chemical equilibrium. We consider a total of sixteen 3D general relativistic radiation hydrodynamics (GRRHD) simulations across equation of state (EOS) models, mass ratios, and grid resolutions. We use the THC.M1 code [13], which implements M1 neutrino transport within the well-established WhiskyTHC code [33, 34] and consider several qualitative and quantitative diagnostics to understand the potential size of out-of-equilibrium effects in the post-merger environment. We find that *the presence of trapped neutrinos implies that not all neutrinos produced during and after the merger efficiently free-stream away from the system. They are instead available for interactions which may drive the matter toward local weak equilibrium.* Although neutrino trapping in BNS mergers with M1 neutrino transport has been previously considered [35], our study provides the first consideration of the potential impact of out-of-equilibrium effects in the post-merger environment using ab-initio simulations with M1 neutrino transport and depicts a nuanced picture of the effects of neutrino interactions in BNS mergers. Unless otherwise noted, we assume natural, geometrized units where $G = c = k_B = 1$.

Methods and Diagnostics.— We consider numerical relativity simulations of 8 binaries with total mass $M = 2.68M_\odot$, mass ratio of either $q = 1$ or $q = 1.2$, and with matter described by 4 microphysical EOS models. The EOS models in our study include BLh [36], DD2 [37], SFHo [38], and SLy4 [39, 40]. The non-rotating, equilibrium neutron stars described by these EOS models are broadly compatible with various astrophysical constraints, including those from massive pulsars [41, 42],

GW170817 [43] and NICER [44, 45]. Simulations are performed by consistently evolving constraint-satisfying initial data in quasi circular orbits through merger. We use the 3+1 Z4c scheme to solve Einstein’s equations [46, 47] coupled to the general relativistic hydrodynamics evolution and the truncated, two-moment M1 gray (energy-integrated) scheme with the Minerbo closure as implemented in the THC_M1 code [13]. The WhiskyTHC code (of which the THC_M1 code is an extension) [13, 32, 48–51] is built upon the Cactus framework [52, 53]. The simulation domain is a cube of side ~ 3024 km centered at the center of mass of the binary system. Within this cube, we consider three nested cubes (two of which track each binary component, while the other is fixed at the computational grid origin) with 7 levels of grid refinement such that the finest-level grid resolution is $\Delta x_{\text{SR}} \approx 185$ m; we refer to simulations with this grid resolution as standard-resolution (SR). To understand the effects of grid resolution, we also consider simulations at a coarser finest-level grid resolution of $\Delta x_{\text{LR}} \approx 247$ m, which we refer to as low-resolution (LR). Ours is the largest-to-date sample of binaries simulated with the M1 neutrino transport scheme and the first consideration of out-of-equilibrium effects using this scheme. The THC_M1 code considers the evolution of three neutrino species including the electron neutrino ν_e , electron anti-neutrino $\bar{\nu}_e$, and a collective species describing heavy flavor neutrinos and antineutrinos ν_x . The set of weak reactions modeled in our simulations is described in detail in [54].

In order to qualitatively understand the potential impact of out-of-equilibrium effects, we consider several post-process diagnostics calculated using the output of our dynamical simulations. For instance, the impact of out-of-equilibrium matter effects in the remnant may be captured by the dimensionless parameter $\mathcal{A} = \mu_{\Delta}/T$ [27], where T is the temperature and μ_{Δ} is the out-of-equilibrium chemical potential. In scenarios where neutrinos stream away on a timescale much smaller than any other relevant timescale and are not expected to be part of the system, the local equilibrium conditions are those of neutrino-less β -equilibrium. As such, the equilibrium value of μ_{Δ} is [27] $\mu_{\Delta}^{npe} \equiv \mu_n - \mu_p - \mu_e$, where μ_i is the chemical potential for species i , and the labels n , p , and e correspond to the neutron, proton, and electron, respectively. In our work, we consider a more accurate measure of the deviation from local weak equilibrium by including trapped electron anti-neutrinos. Specifically, in cases where neutrinos may be significantly trapped, the local equilibrium condition is that of full β -equilibrium, and as such μ_{Δ} becomes $\mu_{\Delta}^{npe\nu} \equiv \mu_n - \mu_p - \mu_e - \mu_{\bar{\nu}_e}$. The chemical potential for the proton, neutron, and electron are provided by the EOS models we employ for each simulation. However, these EOS models do not explicitly account for the impact of neutrinos, and as such we must estimate μ_{ν} using the local neutrino fraction Y_{ν} extracted from our simulations [29]. We note that for the analy-

ses presented in this work we typically consider the electron anti-neutrino fraction, but we find consistent results when considering the electron neutrino fraction with appropriate sign changes instead. We emphasize that our M1 scheme is able to self-consistently evolve the neutrino fraction Y_{ν} and energy u_{ν} , and that electron anti-neutrinos are the most abundant species [16, 35, 54] with typical fractions of $\sim 10^{-3}$ in the relevant high-density regions.

For a complementary look at the potential impact of out-of-equilibrium effects, we also consider the ratio of timescales relevant to bulk viscosity. Specifically, bulk viscosity is expected to emerge as a resonant phenomenon when the timescales of the local compression and rarefaction of the fluid is commensurate with the timescale on which microphysical reactions allows the fluid to reach chemical equilibrium [21–24]. In the case of the environment following a BNS merger, the relevant timescales are those of local density oscillations τ_h and weak interactions τ_{ν} . If these timescales are very disparate, the fluid may undergo adiabatic changes in state variables either so fast that the composition remains effectively fixed ($\tau_{\nu} \gg \tau_h$), or so slowly that it is at all times in chemical equilibrium ($\tau_{\nu} \ll \tau_h$). However, when the two timescales are similar the system may undergo local density oscillations while similarly undergoing local changes in the fluid chemical composition (and thereby local pressure), leading to an emergent dissipation [23, 24].

Results.— In Fig. 1 we show the out-of-equilibrium chemical potential in the equatorial plane of the RMNS for the equal mass ratio, SR simulation with use of the DD2 EOS, at a representative time from merger of $\delta t \approx 3.76$ ms post-merger. The figure shows that matter is not in neutrino-less β -equilibrium, in line with the findings of previous works [26, 27]. As we account for neutrinos in our simulation, we can accurately assess whether or not matter is in neutrino-trapped equilibrium. We find indications of significant neutrino trapping throughout the RMNS, with typical neutrino fractions of $Y_{\nu} \approx 10^{-3}$. As such, an assumption of npe matter is not accurate and regions with high opacity remain near local weak equilibrium [13, 16, 54]. For the sake of brevity, we showcase the results for a single SR simulation, but we find all of our findings to hold regardless of EOS model, mass ratio, and grid resolution.

In Fig. 1 we also show the phase-space histograms, specifically the μ_{Δ} - T plane, for each of the cases depicted in the left panels. The rightmost panel of Fig. 1 corroborates our finding that when neutrino trapping is accounted for, the fluid is driven toward β -equilibrium on timescales that are shorter than the dynamical time [22], thereby potentially reducing the importance of out-of-equilibrium effects. In Fig. 2 we show the ratio of neutrino interaction and density oscillation timescales for the same simulation and timestamp depicted in Fig. 1. We estimate the timescale of local density oscillations as $\tau_h =$

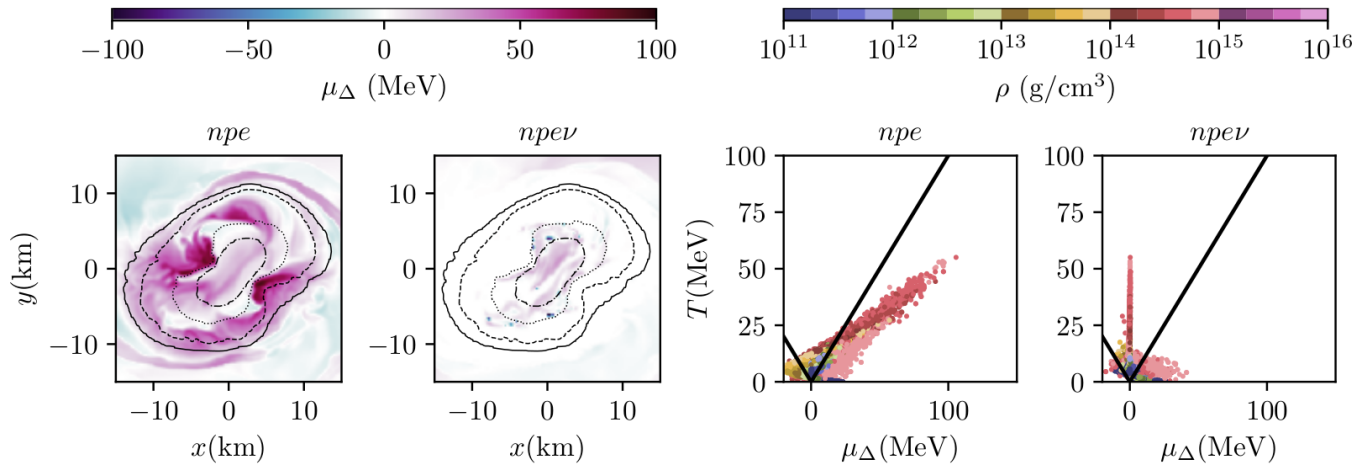


FIG. 1. *Left*: Equatorial snapshots of the out-of-equilibrium chemical potential μ_Δ at a time after the merger of $\delta t \approx 3.69$ ms for the equal mass, SR simulation in our work with use of the DD2 EOS. The leftmost and second-from-left panels depict the case where we assume the matter to consist of npe and $npe\nu$ matter, respectively. We highlight regions in the post-merger environment with rest mass density $\rho = 0.5\rho_{\text{sat}}$, ρ_{sat} , $2\rho_{\text{sat}}$, and $2.5\rho_{\text{sat}}$ (where $\rho_{\text{sat}} \approx 2.5 \times 10^{14}$ g cm⁻³ is the nuclear saturation density) using solid, dashed, dotted, and dash-dotted black lines, respectively. *Right*: Phase-space histograms for the two simulations depicted in the left panel. For these histograms we focus on a time window of ~ 3 ms before and after the merger. We mark the condition where $\mu_\Delta = T$ with solid black lines. Phase-space regions above (below) the solid lines where $T = \mu_\Delta$ imply that the matter is close to (significantly deviating from) weak equilibrium.

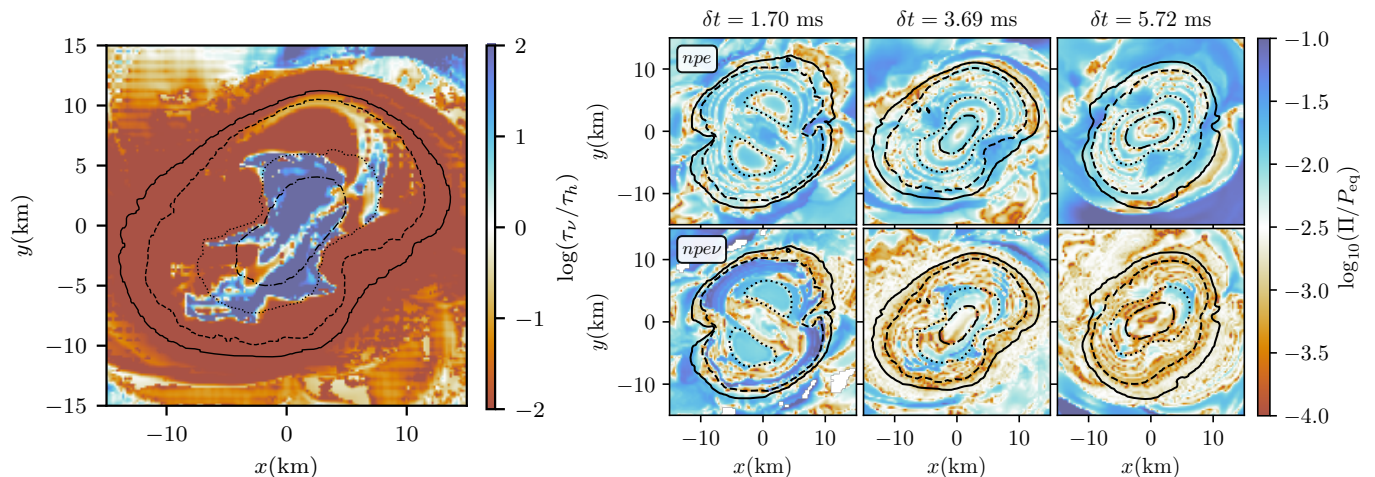


FIG. 2. *Left*: Equatorial snapshot of the ratio of relevant timescales at a time after merger of $\delta t = 3.69$ ms for the same simulation depicted in Fig. 1. Specifically, we show the ratio of the timescale associated with neutrino absorption to that associated with density oscillations. *Right*: Equatorial snapshots of the relative difference between the simulation pressure and the equilibrium pressure $\Pi \equiv |P - P_{\text{eq}}|$ for the same simulation depicted in the left panel. The top panels shows cases where the equilibrium pressure is calculated assuming npe matter (i.e., using the the local electron fraction corresponding to *neutrino-less* β -equilibrium). The bottom panels shows cases where the equilibrium pressure is calculated assuming $npe\nu$ matter, using Eqs. (1)-(2).

$-\nabla_\mu u^\mu \approx D/\dot{D}$, where u^μ is the fluid four-velocity, $D \equiv \rho W \sqrt{\gamma}$, and ρ , W and γ are the rest mass density, Lorentz factor and determinant of the the three-metric, respectively. We estimate the neutrino interaction timescale by considering the local scattering κ_{scat} and absorption κ_{abs} opacities, $\tau_\nu \approx 1/\sqrt{\kappa_{\text{abs}}(\kappa_{\text{abs}} + \kappa_{\text{scat}})}$. Fig. 2 shows that for the majority of the RMNS the neutrino inter-

action timescale is much faster (by at least two orders of magnitude) than the timescale associated with density oscillations. In these regions, neutrino interactions happen rapidly enough to drive the matter toward local weak equilibrium. Figs. 1-2 show regions with significant deviations from weak equilibrium and where the neutrino interaction time is significantly smaller than that associ-

ated with density oscillations. These are likely regions that are in the non-trivial *translucent* regime, which we discuss further below.

For a complementary, quantitative consideration of the deviation from local weak equilibrium, in Fig. 2 we also show the relative difference between the simulation pressure and the pressure corresponding to weak equilibrium $\Pi \equiv P(\rho, T, Y_e) - P_{\text{eq}}(\rho, T^*, Y_e^*)$, where T^* and Y_e^* are the inferred temperature and electron fraction assuming *neutrino-trapped* local weak equilibrium has been established. We infer the local values of T^* and Y_e^* by constructing the neutrino-trapped equilibrium condition in the microcanonical ensemble, which is relevant since matter in BNS mergers is not in a thermal bath but fluid elements have evolutions close to adiabatic. Specifically, we assume that the total energy density u_{sim} and lepton fraction $Y_{\text{lep,sim}}$ extracted from our simulations have contributions from trapped neutrinos [54] such that

$$u_{\text{sim}} = u_{\text{fluid}}(\rho, T^*, Y_e^*) + u_\nu(\rho, T^*, Y_e^*), \quad (1)$$

and

$$Y_{\text{lep,sim}} = Y_e^* + Y_{\nu_e}(\rho, T^*, Y_e^*) - Y_{\bar{\nu}_e}(\rho, T^*, Y_e^*), \quad (2)$$

where u_{fluid} is the energy density of the fluid as interpolated from the EOS model, u_ν is the contribution to the total energy density from trapped neutrinos, and Y_{ν_e} and $Y_{\bar{\nu}_e}$ are the electron neutrino and anti-neutrino fractions, respectively. A root-finding algorithm is then used to solve for T^* and Y_e^* ¹. We do not include the contribution of neutrinos directly on the system pressure, as it is negligible. Instead, the impact of neutrinos emerges as a change on the local relevant matter conditions (namely T^* and Y_e^*) which in turn modifies the fluid pressure to a new equilibrium state. In the case in which we treat the equilibrium condition to be that of *npe* matter, we find typical pressure deviations from equilibrium of $\sim 5\%$ throughout all stages of the post-merger evolution. On the other hand, in cases where we treat the equilibrium state as including trapped neutrinos we generally find smaller deviations from local weak equilibrium, with pressure deviations decreasing by at least an order of magnitude in most regions on a timescale of approximately $\delta t \sim 3$ ms after the merger.

As suggested by Figs. 1-2, there may arise high-density regions in the RMNS that show significant deviations from local neutrino-trapped weak equilibrium, with $\mu_\Delta \sim 10$ MeV, $\tau_\nu \gtrsim 10^2 \tau_h$, and $\Pi/P_{\text{eq}} \sim 0.05$. These are regions where matter is out of equilibrium with neutrinos and neutrinos are also decoupled. We note that in the translucent region neutrinos are trapped due to scattering, so the neutrino-trapped equilibrium is the relevant condition. It is in these translucent regions where

we expect bulk viscosity may arise, as neutrino interactions there are not rapid enough to drive the matter toward equilibrium faster than the local density oscillations (see the *Supplemental Material* for additional diagnostics which support this). However, these regions are spatially small and typically transient, existing only for a few ms after the merger. The majority of the RMNS remains within $\mu_\Delta \lesssim 2$ MeV, with $\tau_\nu \lesssim 10^{-2} \tau_h$, and with $\Pi/P_{\text{eq}} \sim 10^{-3}$ during the most violent stages of the merger, and the entire RMNS evolves toward the condition of neutrino-trapped weak equilibrium on dynamical timescales.

Conclusion.— In this letter we have shown, for the first time using M1 neutrino transport in GRRHD simulations, that neutrinos may remain significantly trapped in the post-merger environment to partake in weak interactions which drive the matter toward weak equilibrium. Our simulations indicate that: (1) if we account for the presence of trapped neutrinos by considering the neutrino fraction Y_ν extracted from our simulations, then the majority of the post-merger system remains within $\mu_\Delta \lesssim 2$ MeV, with only spatially small regions of the remnant *transiently* exceeding these conditions and the RMNS evolving toward $\mu_\Delta = 0$ on dynamical timescales; (2) the neutrino interaction timescale τ_ν is at least two orders of magnitude faster than the timescale for local density oscillations τ_h throughout most of the RMNS, with the aforementioned regions that show significant deviations from $\mu_\Delta = 0$ coinciding with regions that have $\tau_\nu \geq \tau_h$; (3) when considering the matter to consist in part of a trapped neutrino gas, the local deviations from the equilibrium pressure do not exceed $\sim 5\%$ (pressure deviations remain close to $\sim 1\%$ for most of the RMNS) and these deviations decrease toward $\sim 0.1\%$ on dynamical timescales as the RMNS continues to evolve. These analyses show that out-of-equilibrium effects are likely to be small for most of the post-merger evolution, with a possible exception in the translucent region where neutrinos are present but not in thermal or chemical equilibrium with the matter. Our simulation draw a picture of out-of-equilibrium effects in BNS mergers that is much more nuanced than previously anticipated.

The key element in our study is the use of an M1 neutrino transport scheme that does not assume thermodynamic equilibrium between matter and radiation. This allows our simulations to capture the trapping of neutrinos and a more accurate estimate of the chemical potential, relevant timescales, and deviations of the pressure from equilibrium. Our simulations suggest that the post-merger system consists in part of a trapped neutrino gas that keeps the matter near local weak equilibrium. A relatively cheap and effective way of treating this would be to include trapped neutrinos as part of the fluid equation of state. There are potentially other effects that could enhance the bulk viscosity such as the production of thermal pions [27] or muons [55], the presence of hy-

¹ For additional detail on how Y_e^* , T^* , u_ν , Y_{ν_e} and $Y_{\bar{\nu}_e}$ are calculated, we refer the reader to the *Supplemental Material*

perons [56], or high-density deconfinement phase transitions [57, 58], which we do not account for. A consideration of the effects of bulk viscosity would require the modeling of microphysics effects including additional reactions and degrees of freedom. We leave this to future work.

Acknowledgments.— PE acknowledges funding from the National Science Foundation under Grant No. PHY-2020275. PH acknowledges funding from the National Science Foundation under Grant No. PHY-2116686. DR acknowledges funding from the U.S. Department of Energy, Office of Science, Division of Nuclear Physics under Award Number(s) DE-SC0021177, DE-SC0024388, and from the National Science Foundation under Grants No. PHY-2011725, PHY-2116686, and AST-2108467. RG is supported by the Deutsche Forschungsgemeinschaft (DFG) under Grant No. 406116891 within the Research Training Group RTG 2522/1. FZ acknowledges support from the EU H2020 under ERC Starting Grant, no. BinGraSp-714626. LFLM acknowledges funding from the EU Horizon under ERC Consolidator Grant, no. InspiReM-101043372 LL SB acknowledges support from the EU Horizon under ERC Consolidator Grant, no. InspiReM-101043372. SB acknowledges support from the EU Horizon under ERC Consolidator Grant, no. InspiReM-101043372 and from the Deutsche Forschungsgemeinschaft (DFG) project MEMI number BE 6301/2-1. Simulations were performed on Bridges2, Expanse (NSF XSEDE allocation TG-PHY160025), Frontera (NSF LRAC allocation PHY23001), and Perlmutter. This research used resources of the National Energy Research Scientific Computing Center, a DOE Office of Science User Facility supported by the Office of Science of the U.S. Department of Energy under Contract No. DE-AC02-05CH11231. The authors acknowledge the Gauss Centre for Supercomputing e.V. (www.gauss-centre.eu) for funding this project by providing computing time on the GCS Supercomputer SuperMUC-NG at LRZ (allocation pn36ge and pn36jo).

[1] D. Eichler, M. Livio, T. Piran, and D. N. Schramm, *Nature* **340**, 126 (1989).
 [2] M. Ruffert, H. T. Janka, K. Takahashi, and G. Schaefler, *Astron. Astrophys.* **319**, 122 (1997), [arXiv:astro-ph/9606181](https://arxiv.org/abs/astro-ph/9606181).
 [3] S. Rosswog and M. Liebendoerfer, *Mon. Not. Roy. Astron. Soc.* **342**, 673 (2003), [arXiv:astro-ph/0302301](https://arxiv.org/abs/astro-ph/0302301).
 [4] Y. Sekiguchi, K. Kiuchi, K. Kyutoku, and M. Shibata, *Physical Review D* **91** (2015), [10.1103/physrevd.91.064059](https://arxiv.org/abs/10.1103/physrevd.91.064059).
 [5] C. Palenzuela, S. L. Liebling, D. Neilsen, L. Lehner, O. Caballero, E. O’Connor, and M. Anderson, *Physical Review D* **92** (2015), [10.1103/physrevd.92.044045](https://arxiv.org/abs/10.1103/physrevd.92.044045).
 [6] F. Foucart, E. O’Connor, L. Roberts, L. E. Kidder, H. P. Pfeiffer, and M. A. Scheel, *Physical Review D* **94** (2016),

[10.1103/physrevd.94.123016](https://arxiv.org/abs/10.1103/physrevd.94.123016).
 [7] F. Foucart, R. Haas, M. D. Duez, E. O’Connor, C. D. Ott, L. Roberts, L. E. Kidder, J. Lippuner, H. P. Pfeiffer, and M. A. Scheel, *Phys. Rev. D* **93**, 044019 (2016).
 [8] M.-R. Wu, I. Tamborra, O. Just, and H.-T. Janka, *Phys. Rev. D* **96**, 123015 (2017).
 [9] M. George, M.-R. Wu, I. Tamborra, R. Ardevol-Pulpillo, and H.-T. Janka, *Phys. Rev. D* **102**, 103015 (2020).
 [10] A. Burrows, D. Radice, D. Vartanyan, H. Nagakura, M. A. Skinner, and J. Dolence, *Mon. Not. Roy. Astron. Soc.* **491**, 2715 (2020), [arXiv:1909.04152](https://arxiv.org/abs/1909.04152) [astro-ph.HE].
 [11] I. Kullmann, S. Goriely, O. Just, R. Ardevol-Pulpillo, A. Bauswein, and H. T. Janka, *Mon. Not. Roy. Astron. Soc.* **510**, 2804 (2022), [arXiv:2109.02509](https://arxiv.org/abs/2109.02509) [astro-ph.HE].
 [12] M. Cusinato, F. M. Guercilena, A. Perego, D. Logoteta, D. Radice, S. Bernuzzi, and S. Ansoldi, (2021), [10.1140/epja/s10050-022-00743-5](https://arxiv.org/abs/10.1140/epja/s10050-022-00743-5), [arXiv:2111.13005](https://arxiv.org/abs/2111.13005) [astro-ph.HE].
 [13] D. Radice, S. Bernuzzi, A. Perego, and R. Haas, *Mon. Not. Roy. Astron. Soc.* **512**, 1499 (2022), [arXiv:2111.14858](https://arxiv.org/abs/2111.14858) [astro-ph.HE].
 [14] S. Wanajo, Y. Sekiguchi, N. Nishimura, K. Kiuchi, K. Kyutoku, and M. Shibata, *Astrophys. J. Lett.* **789**, L39 (2014), [arXiv:1402.7317](https://arxiv.org/abs/1402.7317) [astro-ph.SR].
 [15] A. Perego, S. Rosswog, R. M. Cabezón, O. Korobkin, R. Käppeli, A. Arcones, and M. Liebendörfer, *Mon. Not. Roy. Astron. Soc.* **443**, 3134 (2014), [arXiv:1405.6730](https://arxiv.org/abs/1405.6730) [astro-ph.HE].
 [16] F. Zappa, S. Bernuzzi, D. Radice, and A. Perego, (2022), [10.1093/mnras/stad107](https://arxiv.org/abs/10.1093/mnras/stad107), [arXiv:2210.11491](https://arxiv.org/abs/2210.11491) [astro-ph.HE].
 [17] B. D. Metzger and R. Fernández, *Mon. Not. Roy. Astron. Soc.* **441**, 3444 (2014), [arXiv:1402.4803](https://arxiv.org/abs/1402.4803) [astro-ph.HE].
 [18] D. Martin, A. Perego, A. Arcones, F.-K. Thielemann, O. Korobkin, and S. Rosswog, *Astrophys. J.* **813**, 2 (2015), [arXiv:1506.05048](https://arxiv.org/abs/1506.05048) [astro-ph.SR].
 [19] A. Perego, D. Radice, and S. Bernuzzi, *Astrophys. J. Lett.* **850**, L37 (2017), [arXiv:1711.03982](https://arxiv.org/abs/1711.03982) [astro-ph.HE].
 [20] D. Radice, A. Perego, K. Hotokezaka, S. A. Fromm, S. Bernuzzi, and L. F. Roberts, *Astrophys. J.* **869**, 130 (2018), [arXiv:1809.11161](https://arxiv.org/abs/1809.11161) [astro-ph.HE].
 [21] A. Schmitt and P. Shternin, *Astrophys. Space Sci. Libr.* **457**, 455 (2018), [arXiv:1711.06520](https://arxiv.org/abs/1711.06520) [astro-ph.HE].
 [22] M. Alford, A. Harutyunyan, and A. Sedrakian, *Phys. Rev. D* **100**, 103021 (2019), [arXiv:1907.04192](https://arxiv.org/abs/1907.04192) [astro-ph.HE].
 [23] G. Camelio, L. Gavassino, M. Antonelli, S. Bernuzzi, and B. Haskell, *Phys. Rev. D* **107**, 103031 (2023), [arXiv:2204.11809](https://arxiv.org/abs/2204.11809) [gr-qc].
 [24] G. Camelio, L. Gavassino, M. Antonelli, S. Bernuzzi, and B. Haskell, *Phys. Rev. D* **107**, 103032 (2023), [arXiv:2204.11810](https://arxiv.org/abs/2204.11810) [gr-qc].
 [25] M. G. Alford, L. Bovard, M. Hanauske, L. Rezzolla, and K. Schwenzer, *Phys. Rev. Lett.* **120**, 041101 (2018), [arXiv:1707.09475](https://arxiv.org/abs/1707.09475) [gr-qc].
 [26] A. Endrizzi, A. Perego, F. M. Fabbri, L. Branca, D. Radice, S. Bernuzzi, B. Giacomazzo, F. Pederiva, and A. Lovato, *Eur. Phys. J. A* **56**, 15 (2020), [arXiv:1908.04952](https://arxiv.org/abs/1908.04952) [astro-ph.HE].
 [27] P. Hammond, I. Hawke, and N. Andersson, *Phys. Rev. D* **104**, 103006 (2021), [arXiv:2108.08649](https://arxiv.org/abs/2108.08649) [astro-ph.HE].
 [28] E. R. Most, A. Haber, S. P. Harris, Z. Zhang, M. G. Alford, and J. Noronha, (2022), [arXiv:2207.00442](https://arxiv.org/abs/2207.00442) [astro-ph.HE].

- [29] L. F. Longo Micchi, D. Radice, and C. Chirenti, *Mon. Not. Roy. Astron. Soc.* **525**, 6359 (2023), [arXiv:2306.04711 \[astro-ph.HE\]](#).
- [30] M. Shibata, K. Kiuchi, Y.-i. Sekiguchi, and Y. Suwa, *Prog. Theor. Phys.* **125**, 1255 (2011), [arXiv:1104.3937 \[astro-ph.HE\]](#).
- [31] F. Foucart, E. O'Connor, L. Roberts, M. D. Duez, R. Haas, L. E. Kidder, C. D. Ott, H. P. Pfeiffer, M. A. Scheel, and B. Szilagyi, *Physical Review D* **91** (2015), [10.1103/physrevd.91.124021](#).
- [32] D. Radice, F. Galeazzi, J. Lippuner, L. F. Roberts, C. D. Ott, and L. Rezzolla, *Mon. Not. Roy. Astron. Soc.* **460**, 3255 (2016), [arXiv:1601.02426 \[astro-ph.HE\]](#).
- [33] D. Radice and L. Rezzolla, *Astronomy and Astrophysics* **547**, A26 (2012).
- [34] D. Radice, L. Rezzolla, and F. Galeazzi, *Monthly Notices of the Royal Astronomical Society: Letters* **437**, L46 (2013).
- [35] F. Foucart, R. Haas, M. D. Duez, E. O'Connor, C. D. Ott, L. Roberts, L. E. Kidder, J. Lippuner, H. P. Pfeiffer, and M. A. Scheel, *Phys. Rev. D* **93**, 044019 (2016), [arXiv:1510.06398 \[astro-ph.HE\]](#).
- [36] I. Bombaci and D. Logoteta, *Astron. Astrophys.* **609**, A128 (2018), [arXiv:1805.11846 \[astro-ph.HE\]](#).
- [37] M. Hempel and J. Schaffner-Bielich, *Nucl. Phys. A* **837**, 210 (2010), [arXiv:0911.4073 \[nucl-th\]](#).
- [38] A. W. Steiner, J. M. Lattimer, and E. F. Brown, *The Astrophysical Journal* **722**, 33 (2010).
- [39] E. Chabanat, P. Bonche, P. Haensel, J. Meyer, and R. Schaeffer, *Nucl. Phys. A* **635**, 231 (1998), [Erratum: *Nucl. Phys. A* 643, 441–441 (1998)].
- [40] A. S. Schneider, L. F. Roberts, and C. D. Ott, *Phys. Rev. C* **96**, 065802 (2017).
- [41] H. T. Cromartie *et al.* (NANOGrav), *Nature Astron.* **4**, 72 (2019), [arXiv:1904.06759 \[astro-ph.HE\]](#).
- [42] E. Fonseca *et al.*, *Astrophys. J. Lett.* **915**, L12 (2021), [arXiv:2104.00880 \[astro-ph.HE\]](#).
- [43] B. P. Abbott *et al.* (Virgo, LIGO Scientific), (2018), [arXiv:1805.11581 \[gr-qc\]](#).
- [44] M. C. Miller *et al.*, (2021), [arXiv:2105.06979 \[astro-ph.HE\]](#).
- [45] T. E. Riley *et al.*, (2021), [arXiv:2105.06980 \[astro-ph.HE\]](#).
- [46] S. Bernuzzi and D. Hilditch, *Phys. Rev. D* **81**, 084003 (2010), [arXiv:0912.2920 \[gr-qc\]](#).
- [47] D. Hilditch, S. Bernuzzi, M. Thierfelder, Z. Cao, W. Tichy, and B. Bruegmann, *Phys. Rev. D* **88**, 084057 (2013), [arXiv:1212.2901 \[gr-qc\]](#).
- [48] D. Radice and L. Rezzolla, *Astron. Astrophys.* **547**, A26 (2012), [arXiv:1206.6502 \[astro-ph.IM\]](#).
- [49] D. Radice, L. Rezzolla, and F. Galeazzi, *Mon. Not. Roy. Astron. Soc.* **437**, L46 (2014), [arXiv:1306.6052 \[gr-qc\]](#).
- [50] D. Radice, L. Rezzolla, and F. Galeazzi, *Class. Quant. Grav.* **31**, 075012 (2014), [arXiv:1312.5004 \[gr-qc\]](#).
- [51] D. Radice, L. Rezzolla, and F. Galeazzi, *ASP Conf. Ser.* **498**, 121 (2015), [arXiv:1502.00551 \[gr-qc\]](#).
- [52] J. A. Font, T. Goodale, S. Iyer, M. A. Miller, L. Rezzolla, E. Seidel, N. Stergioulas, W.-M. Suen, and M. Tobias, *Phys. Rev. D* **65**, 084024 (2002), [arXiv:gr-qc/0110047](#).
- [53] E. Schnetter, C. D. Ott, G. Allen, P. Diener, T. Goodale, T. Radke, E. Seidel, and J. Shalf, (2007), [arXiv:0707.1607 \[cs.DC\]](#).
- [54] A. Perego, S. Bernuzzi, and D. Radice, *arXiv e-prints* (2019), [arXiv:1903.07898 \[gr-qc\]](#).
- [55] E. Loffredo, A. Perego, D. Logoteta, and M. Branchesi, (2022), [arXiv:2209.04458 \[astro-ph.HE\]](#).
- [56] M. G. Alford and A. Haber, *Phys. Rev. C* **103**, 045810 (2021), [arXiv:2009.05181 \[nucl-th\]](#).
- [57] M. G. Alford and K. Schwenzer, *Phys. Rev. Lett.* **113**, 251102 (2014), [arXiv:1310.3524 \[astro-ph.HE\]](#).
- [58] M. G. Alford, S. Han, and M. Prakash, *Phys. Rev. D* **88**, 083013 (2013).

Supplemental Material

Details on the calculation of several post-process diagnostics

As the EOS models which we employ in our study do not account for the presence of trapped neutrinos, we use the conditions extracted from our numerical simulations to infer the neutrino chemical potential used to calculate $\mu_{\Delta}^{npe\nu}$ (see Fig. 1). To do so, we take the following steps:

1. We calculate the Fermi-Dirac integral of order 2, F_2 , using two forms. The first form assumes weak equilibrium and relates F_2 to the neutrino fraction analytically, following [54],

$$F_2(Y_{\nu}) = \frac{\rho(hc)^3}{4\pi m_b(k_B T)^3} Y_{\nu}, \quad (3)$$

where m_b is the baryon mass. Note that Eq. (3) differs from the form used in [54] by an exponential factor which suppresses the impact of neutrinos in low-density regions; we find that this exponential factor does not impact our results, so we opt to remove it for simplicity.

2. We consider another form of F_2 , which considers its standard definition in terms of the neutrino degeneracy parameter η_{ν} ,

$$F_2(\eta) = \int_0^{\infty} \frac{\varepsilon^2 d\varepsilon}{1 + e^{(\varepsilon - \eta_{\nu})}}. \quad (4)$$

3. We evaluate Eq. (4) and interpolate using a finely sampled cubic spline. We then numerically invert the interpolated function to obtain $\eta_{\nu}(F_2)$.
4. We combine Eq. (3) and Eq. (4) to obtain $\eta_{\nu}(Y_{\nu}) = \eta_{\nu}[F_2(Y_{\nu})]$ numerically.
5. We calculate the neutrino chemical potential as

$$\mu_{\nu} = \eta_{\nu}(Y_{\nu})T. \quad (5)$$

The use of Eqs. (3)-(5) to calculate μ_{ν} is most accurate in regions with significant neutrino fractions $Y_{\nu} \gtrsim 10^{-4}$, which we find generally coincide with densities $\rho \gtrsim 10^{12} \text{ g cm}^{-3}$.

In Fig. 2 we show the deviation of the simulation pressure from that under the assumption of local weak equilibrium. The calculation of P_{eq} requires knowledge of the local temperature T^* and electron fraction Y_e^* under the assumption of weak equilibrium, which in turn requires calculation of the contribution of neutrinos to the total system energy density

$$u_{\nu} = \frac{4\pi}{(hc)^3} (k_B T)^4 \left[\frac{7\pi^4}{20} + \frac{\eta_{\nu_e}^2}{2} (\pi^2 + \eta_{\nu_e}^2) \right], \quad (6)$$

and the difference of neutrino and anti-neutrino fractions

$$Y_{\nu_e} - Y_{\bar{\nu}_e} = \frac{4\pi m_b}{3\rho(hc)^3} (k_B T)^3 \eta_{\nu_e} (\pi^2 + \eta_{\nu_e}), \quad (7)$$

where n_b is the baryon number density and $\eta_{\nu_e} = \eta_{\nu_e}(\rho, T^*, Y_e^*)$. In order to calculate T^* and Y_e^* we numerically invert the relationships established by Eqs. (6)-(7) (along with the definitions established in Eqs. (1)-(2)) using Newton-Raphson root-finding. We then calculate $P_{\text{eq}}(\rho, T^*, Y_e^*)$ by interpolating the EOS model pressure to the inferred temperature and electron fraction.

Post-process analyses with different EOS, mass, ratio, and grid resolution

In the main text we showcase results for the equal mass ratio, SR simulation with use of the DD2 EOS. In Fig. 3 we show the ratio of neutrino interaction timescale to density oscillation timescale for the unequal mass ratio, LR simulation with use of the DD2 EOS. We find that, regardless of mass ratio or grid resolution considered, neutrino interactions occur much faster than the local density oscillations. We expect that neutrino interactions occur on the weak interaction timescale $10^{-10} - 10^{-8} \text{ s}$ [27], which is faster than what is resolved in our simulations ($\Delta t \approx 8.22 \times 10^{-8} \text{ s}$ and $\Delta t \approx 6.16 \times 10^{-8} \text{ s}$ for the LR and SR simulations, respectively) and as such we expect the matter to remain close to local weak equilibrium at these resolutions. In Fig. 4 we show several diagnostics which reproduce the results of the main text while varying the

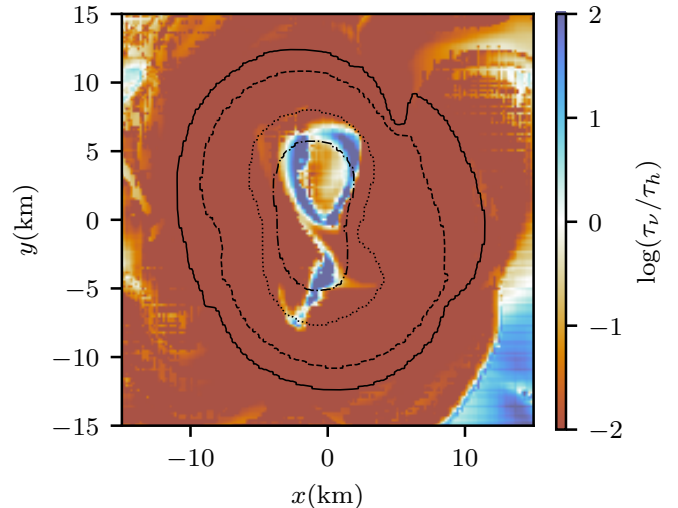


FIG. 3. Equatorial snapshot of the ratio of neutrino interaction timescale to density oscillation timescale for the unequal mass ratio ($q = 1.2$), LR simulation with use of the DD2 EOS. The neutrino interaction timescales are much faster than the timescale of local density oscillations, consistent with result for the equal mass, SR simulation with use of the same EOS (see Fig. 2).

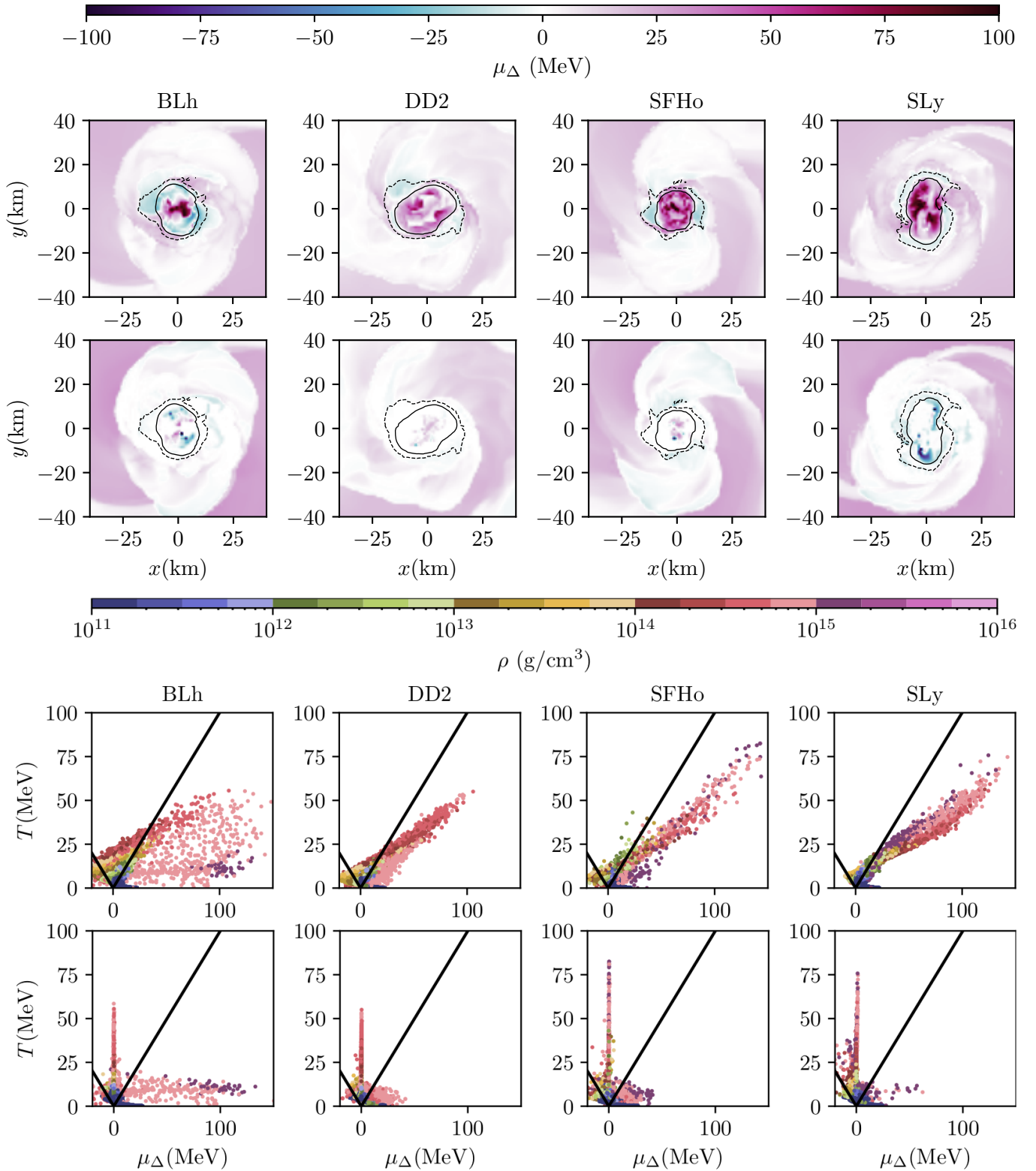


FIG. 4. *Top panels:* Equatorial snapshots of the out-of-equilibrium chemical potential μ_Δ at a time shortly after merger for the equal mass, SR simulations in our work. From left to right, we depict results for simulations which use the BLh, DD2, SFHo, and SLy EOSs. The top panel depicts the approximate chemical potential assuming *neutrinoless* β -decay ($\mu_\Delta^{npe} = \mu_n - \mu_p - \mu_e$). The lower panel includes the contribution from neutrinos ($\mu_\Delta^{npe\nu} = \mu_n - \mu_p - \mu_e - \mu_{\bar{\nu}}$). We highlight regions in the post-merger environment with $\rho \geq 10^{13}$ g/cm³ and $\rho \geq 10^{14}$ g/cm³ using dashed and solid black lines, respectively. *Bottom panels:* Phase-space (μ_Δ - T plane) histograms for the same simulations depicted in the top panels. The colorbar corresponds to the rest mass density. For each simulation we depict the state of matter over a fixed time window of approximately 3 ms before and after the merger. The $\mu_\Delta = T$ condition is shown using a solid black line.

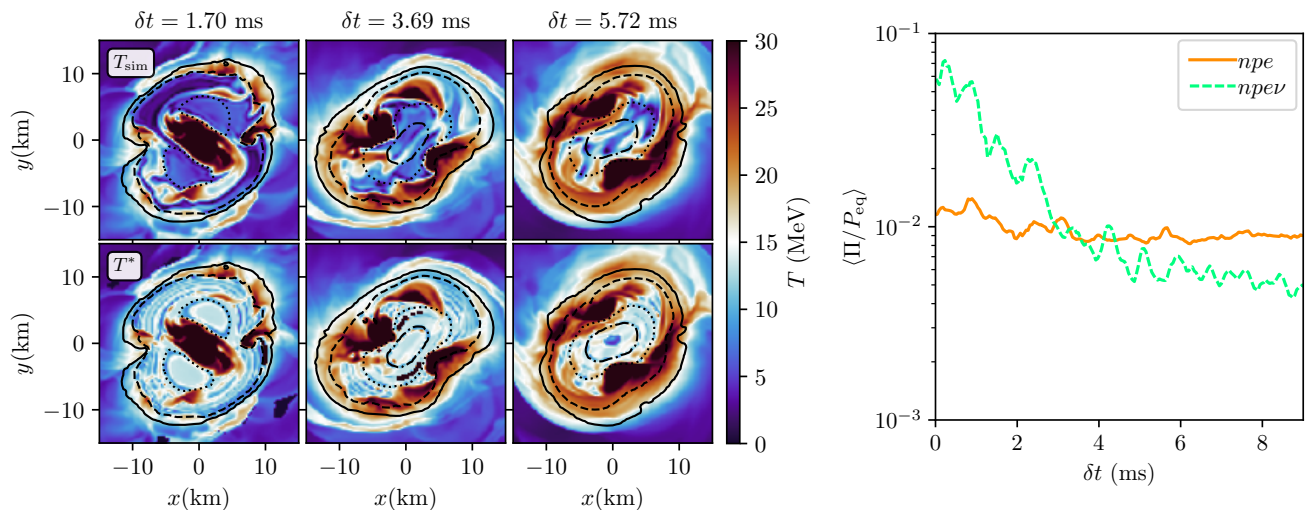


FIG. 5. *Left:* Equatorial snapshots of the simulation pressure T_{sim} (top panels) and the pressure inferred when assuming a trapped neutrino gas T^* (bottom panels) for the equal mass ratio, SR simulation with use of the DD2 EOS (the same simulation depicted in Fig. 1). *Right:* Rest mass density weighted spatial average of the pressure deviation from equilibrium under the assumption of npe (solid orange line) and $npe\nu$ (dashed green line) matter, for the same simulation depicted in the left panel.

EOS. We find that the general results summarized in the *Conclusion* section of the main text hold regardless of EOS. For instance, we find out-of-equilibrium chemical potentials which remain within $\mu_{\Delta} \lesssim 2$ MeV for the majority of the RMNS if we consider the post-merger system to consist in part of a trapped neutrino gas. There are high-density regions in the RMNS which show significant deviations from weak equilibrium. However, for all cases we consider, these regions tend to be small and transient, existing for only a few ms after the merger. We note that not all EOSs we consider lead to long-lived RMNSs for which out-of-equilibrium effects would be most relevant. Nevertheless, we find that the matter is driven toward weak equilibrium on sufficiently fast timescales for out-of-equilibrium effects to potentially be mitigated, regardless of RMNS lifetime.

Additional post-process analyses

For additional analyses to support those presented in the main text, we consider qualitative diagnostics for the equal mass ratio, SR simulation with use of the DD2 EOS. In Fig. 5 we show the temperature extracted from our simulations T_{sim} along with the inferred temperature T^* assuming a neutrino trapped gas, using Eqs. (1)-(2) and Eqs. (6)-(7). When we account for a neutrino trapped gas we note a relative increase in the local tem-

perature in the core of the RMNS. The regions with $T^* > T_{\text{sim}}$ spatially coincide with the translucent regions discussed in the main text and are where we see significant deviations from weak equilibrium as suggested by other diagnostics. The hot regions originating from the shocked interface at the merger are expected to copiously produce neutrinos [16] which inundate the translucent regions. However, the neutrinos produced in hot regions cannot equilibrate due to Pauli blocking which suppresses heat exchange with the neutrino fluid [54]. In Fig. 5 we also show the ρ -weighted spatial average of the pressure deviation from equilibrium as a function of time for the equal mass ratio, SR simulation with use of the DD2 EOS. Fig. 5 shows that in the few ms immediately following the merger, the average deviation from equilibrium is significantly higher if we treat the equilibrium state to be $npe\nu$ matter, mostly due to the fact that the initial conditions for our simulations are for npe matter in equilibrium, consistent with cold neutron stars during the inspiral. We note that the RMNS cores remain cold and close to the initial conditions. As such, the state of the majority of the matter during the inspiral, at the merger, and immediately after the merger is expected to be closer to neutrino-less β -equilibrium. However, within ~ 4 ms after the merger, we find that the fluid pressure deviates significantly less from $npe\nu$ equilibrium than from npe equilibrium, consistent with the picture of significant neutrino trapping.